



## **SIMPLIFIED MODELING OF NON-RECTANGULAR RC STRUCTURAL WALLS**

B. L. Brueggen<sup>1</sup> and C. W. French<sup>2</sup>

### **ABSTRACT**

To facilitate development of performance-based engineering (PBE), a simplified modeling approach was developed for use by structural engineers to predict the load-deformation response of structures incorporating walls. In addition to determining the load-displacement response of walls, it associates predicted strain levels with expected degrees of damage, such as cracks requiring repair, concrete cover spalling, and imminent failure. The predicted load-displacement response is separated into components of deformation due to flexure, shear, and strain penetration to give further indication of types of expected damage, such as flexural or web shear cracks. To investigate the robustness of the model relative to the prediction of the force-deformation response of wall systems, results were compared to the response of several specimens tested by other researchers.

### **Introduction**

The adoption of PBE for buildings incorporating reinforced concrete (RC) structural walls in the lateral force resisting system is hindered by the lack of an appropriate modeling tool. Detailed modeling tools, which have the potential to provide sufficient accuracy to be useful, require significant modeling and computational effort. While these tools can be beneficial to researchers or designers of landmark buildings, they are not appropriate for use in routine design. Conversely, the available simplified tools tend to be grossly conservative, limiting their utility in design of efficient structures. This paper describes a new model, the F-S-SP Integration Model, which seeks to fill this need and provide a reasonably accurate tool for use by designers.

### **Performance-Based Engineering**

Improvements in the understanding and quantification of wall performance are needed to facilitate the use of PBE for seismic regions. A series of documents has been produced outlining the framework for PBE of building structures. Early documents (i.e., FEMA 356, 2000) focused on retrofit of existing buildings, but more recent documents (i.e., FEMA 445, 2006) have been focused on expanding efforts to new construction. These documents seek to establish target performance levels for buildings subjected to selected demand levels. A minimum of four performance levels are considered: Functional, Immediate Occupancy (IO), Life Safety (LS) and

---

<sup>1</sup>Associate II, Wiss, Janney, Elstner Associates, Inc., Irving, TX 75063

<sup>2</sup>Professor, Dept. of Civil Engineering, University of Minnesota, Minneapolis, MN 55455

Collapse Prevention (CP), and four earthquake hazard levels ranging from frequent (probability of exceedance 50 percent in 50 years) to very rare (2 percent in 50 years) are considered. The minimum acceptable performance levels for ordinary (Seismic Use Group I) buildings are life safety during the 10 percent in 50 year event and collapse prevention during the 2 percent in 50 year event. This is analogous to the current prescriptive design requirement. However, the expanded framework of PBE allows owners to specify enhanced behavior, such as immediate occupancy after frequent earthquakes, potentially reducing costs over the life of the building.

In order to successfully meet these enhanced performance goals and to quantify the expected economic benefits of using them, adequate tools are necessary to predict both the likely demands on the structure and the expected performance of the structure under these demands.

### **Existing Tools**

FEMA 356 (2000) recommends a simplified modeling approach for use with existing buildings. The document provides effective flexural stiffness values, and users are instructed to calculate component stiffnesses considering the effects of shear, flexure, axial behavior and reinforcement slip deformations. In determining the capacity of the wall and the expected degree of damage, only resistance at first yielding and axial load ratio are used. This model is often considered excessively conservative, yet its reliability has not been investigated, discouraging engineers from using it (Hamburger 1997).

Hines *et al.* (2004) developed a simplified, semi-empirical model for determining the force-displacement relationship for rectangular and hollow box-shaped bridge piers with confined corner elements. This model extends existing empirical models to estimate plastic hinge length and rotation in RC members by adding terms describing the deformations due to shear and strain penetration to those describing flexural deformations. This model is not well-suited for use with building structures. It is limited to the analysis of prismatic cantilevers with a point load at the tip and cannot be used to determine interstory displacements.

Prediction of repair costs and downtime after earthquake events requires the linking of defined performance levels, damage states, and likely repair requirements to engineering demand parameters (EDPs) that can be determined from structural analysis. Previous work (FEMA 356 2000, Berry *et al.* 2008) has considered the use of both deformation- or drift-based EDPs and local EDPs, such as strain. While both approaches have been found to be reliable, the use of local EDPs provides a better description of the expected damage level (Berry *et al.* 2008).

The selection of appropriate EDPs and damage measures for various performance levels is ongoing. FEMA 356 (2000) represents an early effort in defining limits for the IO, LS, and CP performance levels. In this model, the performance level is linked to drift, but the repairs likely to be required at each performance level are not specifically identified.

More recent efforts have refined the definitions of performance levels and have correlated more specific damage measures with the general performance levels. Many have expanded the number of performance and damage levels defined. Pagni and Lowes (2006) recommend 12 discrete damage levels for RC beam-column joints. These damage levels range from initial hairline cracking to crushing of the concrete core and reinforcement failure. Berry *et al.* (2008) determined that these damage levels are appropriate for describing the damaged condition of reinforced concrete structural elements in general and selected four of these damage levels (i.e., minimum/IO, minimal, moderate/LS, and significant/CP) as the most important for predicting

repair costs and downtime for PBE of RC columns. These four damage levels were correlated with local EDPs, although critical values for the proposed local EDPs were not provided.

### **F-S-SP Integration Model**

The F-S-SP Integration Model was developed to predict the lateral-load deformation response of structures incorporating slender shear walls. The model describes deformations due to flexure, shear, and strain penetration based on a flexural section analysis, which can be generated using readily available software such as BIAX (Wallace 1992). The flexural behavior of the wall is used as the basis for the entire model because flexure is the most well-understood and most predictable component of the total deformation, besides being the dominant deformation component for cantilever walls. The following sections describe the development of each term of the F-S-SP Integration Model.

For illustration purposes, the model is applied to a cantilever wall specimen, NTW1, tested by the authors (Brueggen 2009) in the web direction. The specimen consisted of a one-half scale T-wall that represented the lower four stories of a six-story prototype. Detailing of the specimen was generally in accordance with ACI 318-02 requirements for special RC walls, which were current at the time of construction. Figure 1 shows a lower-level cross section of the wall, including the provided confining reinforcement.

The load deformation behavior predicted by the F-S-SP Integration model represents the backbone response. It does not capture premature failures such as reinforcement fracture due to reinforcement elongation following buckling in compression during reversed-cyclic loading. It should be noted that this type of premature failure was observed in the flange-in-compression loading direction of NTW1.

### **Flexural Component of Deformation**

The flexural component of deformation is calculated directly from the moment-curvature relationship determined from a sectional analysis. As the geometry and reinforcing of the wall may change over its height, different sectional analyses can be conducted for each configuration. For a given applied load, the moment distribution over the height of the wall is calculated. The moment-curvature relationships determined from the sectional analyses are then used to determine the distribution of curvature over the height of the wall for the various load cases. Lateral displacements can be determined by integrating the curvature distribution over the height of the wall twice. This approach neglects the effects of diagonal cracking and tension shifting, which can increase the effective plastic hinge length. As a result, there is a tendency to underestimate flexural deformations in the inelastic range with this approach.

Figure 2 compares the measured and predicted relationship between load and displacement due to flexural deformation for specimen NTW1 in the web direction. As mentioned above, the model considers only monotonic loading. The model predicted a much larger curvature capacity than measured in the flange-in-compression loading direction, with failure not expected to occur until the reinforcement ruptures at a very large curvature level.

As a result of neglecting the increase in plastic hinge length in the model associated with diagonal cracking-related tension shift, the plastic hinge rotation at failure in the flange-in-tension loading direction was underpredicted. However, the load capacity was predicted within 2 percent of the measured value. It should be noted that the tendency to underestimate

deformation capacity at failure is conservative.

### Shear Component of Deformation

Prediction of shear deformations is complicated because flexural damage leads to increased shear deformations. At large ductility levels, large shear and flexural deformations are concentrated in the plastic hinge region. This behavior is observed even in the case of cantilever walls subjected to a constant shear demand over the height (i.e., case of a single concentrated lateral load applied at the top of the wall). Examination of test results from Brueggen (2009), Johnson (2007) and Hines (2002) indicated that the shear strain distribution over the wall height was approximately proportional to the curvature distribution. This relationship can be expressed as  $\gamma=C*\phi$  or as  $\Delta_{\text{shear}}=C*\theta_f$ , where the second expression is obtained by integrating both sides of the first relation over the height of the wall. In these expressions,  $\gamma$  is the shear strain,  $\phi$  is the curvature,  $\Delta_{\text{shear}}$  is the cumulative shear deformation,  $\theta_f$  is the rotation due to flexure, and  $C$  is the proportionality constant with units of length.

Because the proportional relationship between shear strain and curvature is assumed to be constant over the entire range of loading, predictions of the shear and flexural stiffness at first yielding can be used to determine a rational value of  $C$ . The flexural section analysis predicts the flexural stiffness at yielding. Using a truss model and neglecting shear-flexure interaction, Park and Paulay (1975) derived the theoretical cracked shear stiffness  $K_v$  of a RC member with cracks inclined at a  $45^\circ$  angle and shear reinforcement perpendicular to longitudinal reinforcement as  $K_{v45} = \rho_v E_s b_w d / (1 + 4n\rho_v)$ , where  $\rho_v$  is the ratio of shear reinforcement area to the gross area of concrete perpendicular to that reinforcement,  $n$  is the ratio of the elastic modulus of steel to the elastic modulus of concrete,  $E_s$  is the elastic modulus of steel,  $b_w$  is the width of the concrete web, and  $d$  is the depth from the extreme compression fiber to the centroid of the longitudinal tension reinforcement.

Taking the ratio of the flexural stiffness at yielding to the cracked shear stiffness leads to a constant with units of length squared, while the desired constant has units of length. Multiplying the shear stiffness by the shear span,  $z$ , leads to  $C = (M_y/\phi_y)/(K_v z)$ . In this expression,  $M_y$  and  $\phi_y$  are the moment and curvature at first yielding, as predicted by the flexural model,  $K_v$  is the cracked shear stiffness, defined above for the case with cracks inclined at a  $45^\circ$  angle. The shear span was chosen for this factor because it is a representative length relating shears and moments, and was found to give reasonable results for specimens NTW1 and NTW2 tested by Brueggen (2009). For nonsymmetric walls, different values of  $C$  must be calculated for each loading direction.

Figure 3 compares the measured and predicted web direction shear deformations. In the flange-in-compression loading direction, the predicted shear response is stiffer than the measured response at all load levels. This result is primarily associated with the predicted flexural response being stiffer than the measured. In the flange-in-tension loading direction, the predicted shear response is less stiff than the measured. This result is primarily associated with the assumption that diagonal cracks would be oriented at a  $45^\circ$  angle, while the observed cracks in the specimen were steeper. The model can be calibrated to better fit measured data by setting the inclination of diagonal cracks equal to the observed crack orientation. Because tools to predict the angle of diagonal cracks do not currently exist, this calibration is not available for true prediction.

## Strain Penetration Component of Deformation

The approximation of deformations due to strain penetration is based on the assumption that plane sections remain plane, so that the rigid body rotation of a wall due to strain penetration can be calculated based on the slip of the extreme tensile bars and the neutral axis location. The neutral axis location is readily determined from the flexural section analysis, and the slip of the extreme tension bar(s) can be determined using any desired method, such as Lowes and Altoontash (2003).

A reasonable estimation of the slip can be obtained with minimal computational effort by introducing two additional simplifying assumptions into the model proposed by Lowes and Altoontash (2003): 1) the anchorage length,  $l_a$ , over which the bar stress was assumed to be distributed, is calculated at the yield stress and assumed to be constant regardless of the applied bar stress, rather than increasing with the applied stress, and 2) the strain gradient is assumed to be constant over the anchorage length for a particular applied stress, rather than becoming nonlinear in any portions of the reinforcement that have yielded. The second assumption neglects both the decreased modulus of the reinforcement and the decreased bond stress that is observed in any portions of the reinforcement that have yielded.

Assuming a constant bond stress of  $\tau_{avg}=0.67\sqrt{f_c}$  (ksi) or  $1.75\sqrt{f_c}$  (MPa) as recommended by Eligehausen *et al.* (1983), the anchorage length  $l_a$  at yielding is calculated as  $l_a=(3/8)f_y/\sqrt{f_c}$  (ksi)  $= (1/7)f_y/\sqrt{f_c}$  (MPa). Using constant anchorage length for all applied stresses and assuming a triangular strain distribution leads to an approximation of  $\delta_{slip}=0.5\varepsilon_{base}l_a$ , where  $\varepsilon_{base}$  is the strain in the extreme tensile steel at the base of the wall for a given loading, which can be obtained from the flexural section analysis. Assuming small angles, the rigid body rotation due to strain penetration,  $\theta_{sp}$ , is then approximated as  $\theta_{sp}=\varepsilon_{base}l_a/[2(d-c)]$ , where  $d$  is the distance from the extreme compression fiber to the extreme tensile steel and  $c$  is the neutral axis depth.

Figure 4 compares the measured rotations due to strain penetration in specimen NTW1 under web direction loading to the rotations predicted using the F-S-SP model. The measured rotations were obtained from measurements of length change between small studs welded to longitudinal reinforcing bars and the surface of the concrete foundation block. Additional details about this measurement can be found in Brueggen 2009. Contrary to the expected tendencies of the simplified strain penetration model, the strain penetration after yielding in the flange-in-tension loading direction was overpredicted. One possible source of this discrepancy was the location of the stud used to measure bar slip in the flange, which made separating deformations due to strain penetration from flexural deformations difficult.

## Combined Response

Figure 5 compares the measured total response of the specimen with the prediction created by summing the predicted values for each of the three components of deformation. As evident in the figure, the stiffness prior to yielding was overpredicted. This error was largely caused by the flexural section analysis indicating that cracking would be limited to the first story of the specimen at this point in the loading history, while cracking was observed over a larger portion of the specimen in the laboratory. Neglecting the tensile capacity of the concrete (i.e., assuming that the section was initially cracked) addresses this issue and reduces unconservative errors in predicting damage under small loads. Additionally, the displacement at failure was overpredicted in the flange-in-tension loading direction. This is notable because the F-S-SP

Integration Model is expected to underpredict deformations at failure due to neglecting tension shifting. In this particular specimen, premature failure occurred when confining steel pulled out of the concrete core in the web tip, limiting the compression strain capacity of the confined core.

## Validation

The F-S-SP Integration Model was applied to several wall and pier specimens and evaluated based on its ability to predict the initial stiffness, failure mode, maximum moment capacity, and deformation capacity of each specimen. The results are summarized in Table 1. Measured material properties, as reported by the respective researchers, were used for validation. Because the F-S-SP Integration model is capable of predicting deformations at any location on the height of a wall, comparisons were made between measured displacements taken near the top of the physical specimens NTW1 and NTW2 and predicted values at the same height.

Table 1. Percent differences\* between measured and predicted responses.

Specimen	Loading Direction	Stiffness @ first yielding	Maximum Shear	Displacement @ max. shear	Displacement @ Failure
NTW1 (Brueggen 2009)	Flange Direction	18%	-3%	-12%	-20%
	Flange in Tension	-7%	2%	12%	11%
	Flange in Compression	61%	**	**	**
NTW2 (Brueggen 2009)	Flange Direction	94%	-3%	-34%	-28%
	Flange in Tension	-17%	0.2%	24%	-5%
	Flange in Compression	-10%	**	**	**
RWN (Johnson 2007)	No. 9 in Tension	13%	5%	5%	-15%
	No. 9 in Compression	30%	**	**	**
TW2 (Thomsen & Wallace 1995)	Flange in Tension	17%	3%	-73%	-73%
	Flange in Compression	-5%	**	**	**
CMS (Sittipunt & Wood 1995)	Flange in Tension	-8%	1%	-48%	-43%
	Flange in Compression	30%	**	**	**
3A (Hines 2002)		60%	3%	6%	6%
LPT (Hines 2002)		20%	-7%	-17%	-23%

\*Percent differences were taken as  $[(\text{Measured}-\text{Predicted}) / \text{Measured}] \times 100$

\*\* Failure was not reached in laboratory

## Prediction of Damage States for Performance Based Engineering

The descriptions of damage thresholds and associated local engineering demand parameters (EDPs) for RC columns proposed by Berry *et al.* (2008) were adopted as a framework for predicting damage states for RC structural walls in this study. While there are some pertinent differences between structural walls and columns, the significant damage states and related local EDPs recommended by Berry *et al.* (2008) are generally appropriate for describing the damage states of walls and the associated need for repair.

Critical values for the local EDPs were determined based on the measured crack widths and observed damage to the cover and core concrete throughout the testing of specimens NTW1 and NTW2 (Brueggen 2009). The recommended values for each EDP are summarized in Table 2. These values can be applied in design by comparing strains predicted using the F-S-SP Integration model or other tools to the threshold values. In this table, the first four columns represent the framework proposed by Berry *et al.* (2008). The last column contains new

threshold values of the EDPs calibrated for half-scale wall specimens. It should be noted that during the testing, observations of crack widths and concrete spalling were made only at ramp peaks and points of zero load. As a result, correlations between observed damage and each of the local EDPs can only be made at discrete points in the loading history, and critical values of the EDPs for the specimens can be given bounds but not described precisely. It is also notable that these values are based on testing of one-half scale specimens, with reduced clear cover relative to full-size walls. Because crack widths are known to increase with cover (ACI 318-02), comparison of these critical EDP values to results of full-size tests may require revision.

It is recommended that “failure” due to crushing of the confined core be identified when the flexural analysis indicates that the flexural resistance has decayed to some fraction (e.g., 90 percent) of the maximum resistance, rather than imposing an arbitrary, fictitious maximum strain on the extreme compression fiber. This method depends on the selected confined concrete model accurately representing the descending branch of the material behavior, but it is less sensitive to member geometry than the use of a maximum compression strain to define failure.

Because a limited amount of data was used to determine the guidelines in Table 2 and large scatter has been observed in historical data, particularly regarding crack widths (ACI 318-02, Pagni and Lowes 2006), the given thresholds should be considered approximate and are likely to be revised as additional tests are carried out and additional data is used for calibration.

Figure 6 compares the measured response of specimen NTW1 to predictions based on the FEMA 356 (2000) and F-S-SP Integration models. The F-S-SP Integration Model represents the specimen behavior with much greater accuracy. The FEMA 356 model provides conservative estimates of the ultimate load and displacement capacities, but it results in an unconservative estimate of the drift level associated with life safety performance in the flange-in-tension loading direction.

Table 2. Recommended threshold values for EDPs

Damage Level	FEMA 356 Perf. Level	Required Repair	Local EDP	Threshold Value
Negligible		None	Reinforcing steel tensile strain	$\epsilon_s < 3.5\epsilon_y$ , conc. steel*
				$\epsilon_s < 7\epsilon_y$ , dist. steel*
Minimum	Immediate Occupancy	Epoxy injection of cracks	Reinforcing steel tensile strain	$\epsilon_s > 3.5\epsilon_y$ , conc. steel
				$\epsilon_s > 7\epsilon_y$ , dist. steel
Minimal		Patching of concrete cover and epoxy injection of cracks	Cover concrete compressive strain	$\epsilon_c > 2f'_c/E_c$ or 0.003
Moderate	Life Safety	Replacement of concrete cover and epoxy injection of cracks	Core concrete compressive strain	$\epsilon_c > 4kf'_c/E_c$ **
Significant	Collapse Prevention	Replacement of section	Post-peak loss of capacity	

\*Conc. steel indicates longitudinal reinforcement concentrated in boundary elements with minimal longitudinal reinforcement elsewhere. Dist. steel indicates longitudinal reinforcement uniformly distributed across wall element.

\*\* $kf'_c$  is expected compressive strength of confined core, determined using Modified Kent & Park or other appropriate model.

Because a limited amount of data was used to determine the guidelines in Table 2 and large scatter has been observed in historical data, particularly regarding crack widths (ACI 318-02, Pagni and Lowes 2006), the given thresholds should be considered approximate and are likely to be revised as additional tests are carried out and additional data is used for calibration.

Figure 7 compares the measured response of specimen NTW1 to predictions based on the FEMA 356 (2000) and F-S-SP Integration models. The F-S-SP Integration model represents the specimen behavior with much greater accuracy. The FEMA 356 model provides very conservative estimates of the ultimate load and displacement capacities, but it provides an unconservative estimate of the drift level associated with the Life Safety performance level in the flange-in-tension loading direction.

### Conclusions

A simplified model, the F-S-SP Integration Model, was developed to facilitate PBE of rectangular and non-rectangular concrete structural walls. Unlike previous models, this model accounts for each mode of deformation (i.e. flexure, shear, and strain penetration) individually. Additionally, it is capable of determining deformations at any location over the height of a wall and can be used to model walls with variations in section or multiple loads along the height.

The F-S-SP Integration Model has been validated using the results of eight tests of walls and bridge piers. Four of these tests were completed by the authors and four were selected from the literature. The model was also compared to two existing simplified models (FEMA 2000 and Hines *et al.* 2004) and found to describe the load-displacement response more accurately than either.

In addition to predicting the load-displacement relationships for reinforced concrete structural walls, recommendations are made to predict significant damage levels and required repairs based on the expected loading. While these recommended values are expected to be revised based on the results of additional tests of walls, they provide a baseline for engineers to estimate the extent of repairs that will be required after a seismic event of a given magnitude. This allows the engineer to estimate the required repairs and associated costs in order to provide the life-cycle cost estimates required for performance-based engineering.

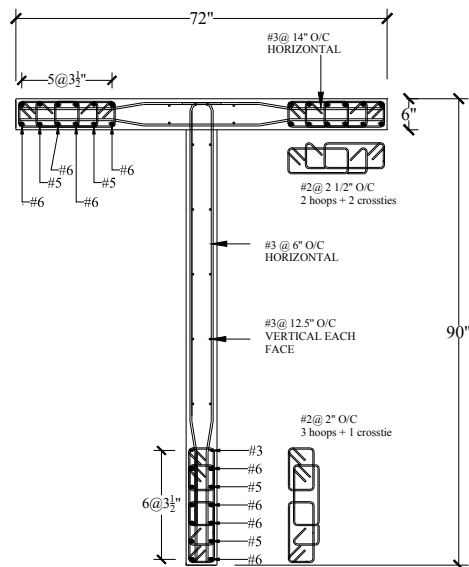


Figure 1. Section of NTW1 (first story).

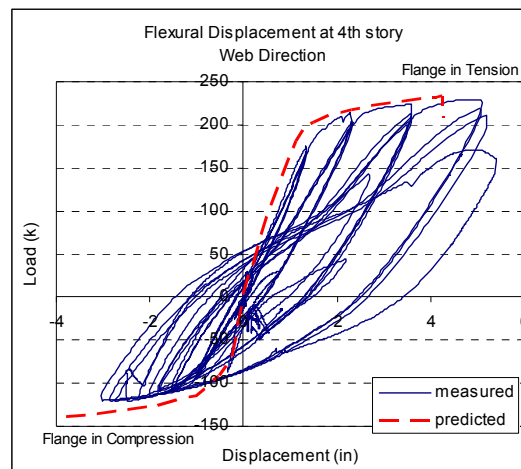


Figure 2. Measured and predicted lateral load vs. Flexural displacement.

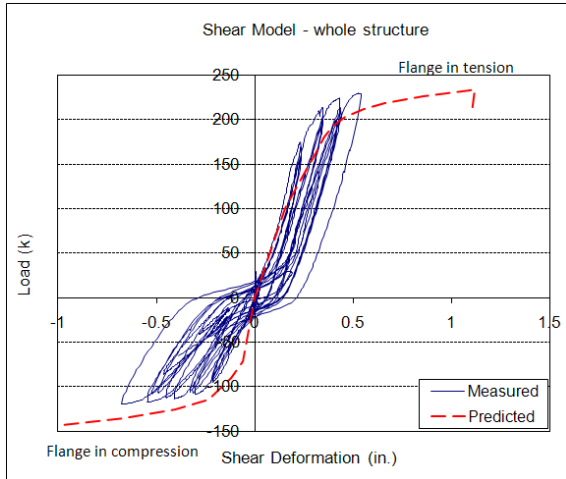


Figure 3. Measured and predicted lateral load vs. shear deformation.

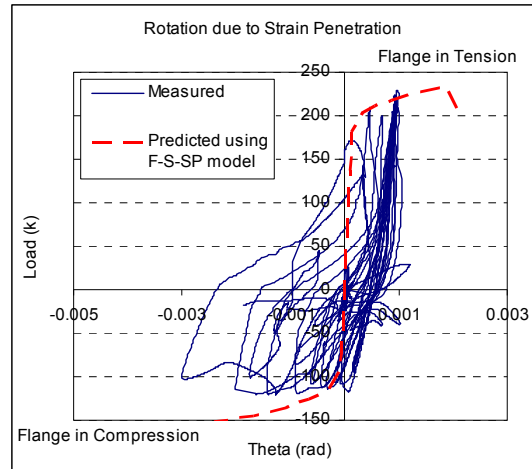


Figure 4. Measured and predicted lateral load vs. rotation due to strain penetration.

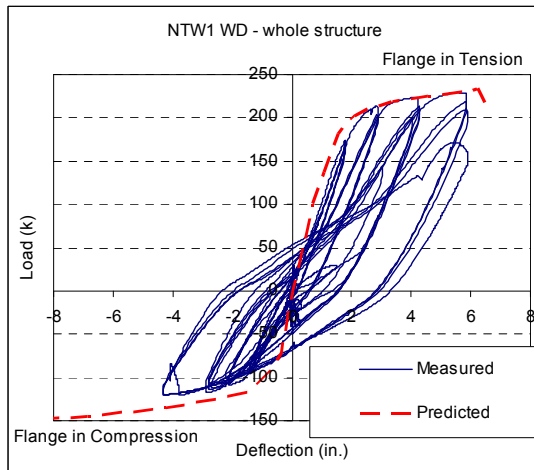


Figure 5. Comparison of measured and predicted total responses.

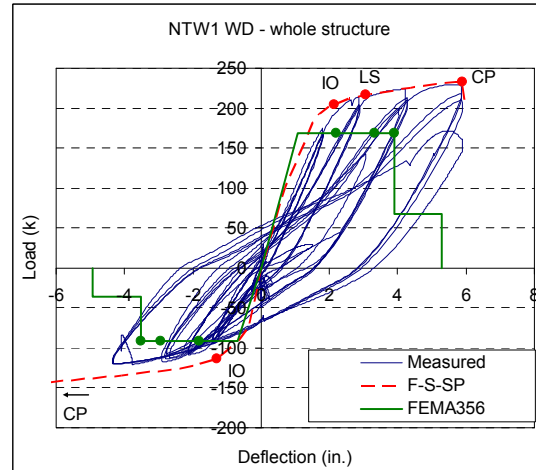


Figure 6. Comparison of F-S-SP Integration and FEMA 356 simplified models.

## Acknowledgments

This research was completed under grant CMS 0324504 from the National Science Foundation. The views expressed in this paper reflect those of the authors.

## References

- ACI Committee 318, 2002. *Building Code Requirements for Structural Concrete (ACI 318-02)*, American Concrete Institute, Farmington Hills, MI.
- Berry, M.P., Lehman, D.E., and Lowes, L.N., 2008. "Lumped-Plasticity Models for Performance Simulation of Bridge Columns," *ACI Structural Journal* 105 (3), pp. 270-279.
- Brueggen, B.L., 2009. *Performance of T-shaped Reinforced Concrete Structural Walls under Multi-Directional Loading*, Ph.D. Thesis, University of Minnesota, Minneapolis.

- Eligehausen, R., Popov, E.P., and Bertero, V.V., 1983. *Local Bond Stress-Slip Relationships of Deformed Bars under Generalized Excitations*, Report. No. UCB/EERC-83/23 EERC, Univ. of California, Berkeley, CA, 162 pp.
- Federal Emergency Management Agency, 2000. *Prestandard and Commentary for the Seismic Rehabilitation of Buildings (FEMA 356)*, Federal Emergency Management Agency, Washington, DC.
- Hamburger, R.O., 1997. "Contributions of earthquake reconnaissance to improved understanding of seismic behavior and performance of buildings," *Structures Congress Proceedings* 1, pp. 639-644.
- Hines, E.M., 2002. *Seismic Performance of Hollow Rectangular Concrete Bridge Piers with Confined Corner Elements*, Ph.D. Thesis, University of California, San Diego, CA, 312 pp.
- Hines, E.M., Restrepo, J.I., and Seible, F., 2004. "Force-Displacement Characterization of Well-Confined Bridge Piers," *ACI Structural Journal* 101 (4), pp. 537-548.
- Johnson, B.M., 2007. *Longitudinal Reinforcement Anchorage Detailing Effects on RC Structural wall Behavior*, M.S. Thesis, University of Minnesota, 391 pp.
- Lowes, L., and Altoontash, A., 2003. "Modeling Reinforced Concrete Beam-Column Joints Subjected to Cyclic Loading," *Journal of Structural Engineering*, 129 (12), pp. 1686-1697.
- Park, R., and Paulay, T., 1975. *Reinforced Concrete Structures*, John Wiley and Sons, New York.
- Sittipunt, C., and Wood, S.L., 1995. "Influence of Web Reinforcement on the Cyclic Response of Structural Walls," *ACI Structural Journal*, 92 (6), pp. 1-12.
- Thomsen, J. H., IV, and Wallace, J. W., 1995. *Displacement-Based Design of RC Structural Walls: Experimental Studies of Walls with Rectangular and T-shaped Cross Sections*, Report No.CU/CEE-95/96, Department of Civil and Environmental Engineering, Clarkson University, 353 pp.
- Wallace, J.W., 1992. *BIAX: Revision 1 – Computer Program for the Analysis of Reinforced Concrete and Reinforced Masonry Sections*, Report CU/CEE-92/4, Structural Engineering, Mechanics, and Materials, Clarkson University, Potsdam, NY.